

Commun. Theor. Phys. **75** (2023) 065601 (11pp) https://doi.org/10.1088/1572-9494/accf04

Interactions between amphiphilic nanoparticles coated with striped hydrophilic/hydrophobic ligands and a lipid bilayer

Lijuan Sun[1], Yu Cao[1], Xiaojie Chen[2] and Qing Liang[1,*]

[1] Department of Physics and Key Laboratory of Solid Optoelectronic Devices of Zhejiang Province, Zhejiang Normal University, Jinhua 321004, China
[2] Department of Industrial Automation, Guangdong Polytechnic College, Zhaoqing 526100, China

E-mail: qliang@zjnu.edu.cn

Received 27 February 2023, revised 19 April 2023
Accepted for publication 21 April 2023
Published 7 June 2023

Abstract

Due to their unique physicochemical properties, nanoparticles play an important role in the fields of nanomedicine and so on. In this paper, the interactions between the nanoparticles coated with striped hydrophilic and hydrophobic ligands and a lipid bilayer are investigated by using the coarse-grained molecular dynamics simulation. This study focuses on the effects of the density of the ligands, the ratio of the hydrophilic ligands to the hydrophobic ligands, and the rigidity of the ligands on the interactions of the nanoparticles with the lipid bilayer. The results show that the nanoparticles interact with the lipid bilayer in two different ways. The nanoparticle with a small size, a large ratio of hydrophilic ligands to the hydrophobic ligands, and flexible ligands can readily be inserted into the lipid bilayer, and the nanoparticle rotation is very crucial to the insertion of the nanoparticle into the bilayer. However, the nanoparticle with a large size, a small ratio of hydrophilic ligands to hydrophobic ligands, and rigid ligands can only be adsorbed on the surface of the lipid bilayer. This work provides an effective method to modulate the interactions of the amphiphilic nanoparticles with the lipid bilayers and some insights into the applications of the nanoparticles in drug delivery, cell imaging, etc.

Keywords: biomembrane, nanoparticle, molecular dynamics, interaction

(Some figures may appear in colour only in the online journal)

1. Introduction

Nanoparticles (NPs) are particles with at least one-dimensional size in the range of 1–100 nm [1]. They have large surface area to volume ratio, excellent photothermal properties, and so on, and play important roles in fields such as drug delivery, cell imaging, etc [1–5]. According to their chemical composition, NPs can be divided into polymeric NPs, liposomal nanocarriers, inorganic NPs, etc [1, 6]. Polymeric NPs and liposomal nanocarriers usually have good biocompatibility [7, 8], whereas inorganic NPs have good electrical, optical, and magnetic properties and excellent stability in living organisms [1, 9]. In particular, gold NPs (AuNPs) are widely used in photothermal therapy and medical imaging due to their facile synthesis and excellent stability [10–13]. However, inorganic NPs usually have significant cytotoxicity [6, 14–17]. Therefore, how to reduce the cytotoxicity and enhance the biocompatibility of inorganic NPs and how to modulate the interaction of NPs with the cellular membranes are great challenges for the applications of NPs in nanomedicine.

For NPs, the surface property is a key factor determining their interaction with cell membranes. In recent years, a large number of experimental and simulation studies have been devoted to understanding the interactions of NPs coated with

* Author to whom any correspondence should be addressed.

various ligands with lipid bilayers and further revealing the microscopic mechanisms of cytotoxicity of NPs [18–23]. It has been shown that the charge property and the hydrophobicity of the NP surface are two crucial factors influencing the interactions between NPs and the lipid bilayers [24–27]. NPs coated with hydrophobic or positively charged ligands can easily disrupt the structure of cell membranes, causing pore formation in the membranes and exhibiting strong cytotoxicity. Moreover, these NPs can directly translocate across the cell membranes without causing membrane deformation. On the contrary, NPs with electrically neutral or negatively charged surfaces have less influence on the cell membrane structure and are less cytotoxic, and they translocate across the membrane mainly by endocytosis. Therefore, changing the hydrophobicity and the charge property of the ligands coated on the surfaces of the NPs is an effective method to reduce the cytotoxicity of the NPs and modulate the translocating pathway of the NPs across cell membranes.

Our previous molecular dynamics simulations have shown that the interactions of the AuNPs coated with uniform ligands with the liquid-ordered/liquid-disordered domains in the phase-separated lipid bilayers can be readily modulated through changing the ligand density and the ratio of charged ligands to neutral ligands [28]. In addition, Van *et al* compared the translocation of the NPs coated with random ligands and the NPs coated with striped ligands across lipid bilayers and found that the NPs coated with striped ligands can more easily translocate across the lipid bilayers [29, 30]. Recently, Lee *et al* experimentally investigated the interaction of amphiphilic Janus NPs with different ratios of hydrophilic to hydrophobic surface with lipid bilayers. The results showed that when the hydrophobic surface area exceeds 20% of the total surface area of the NP, the NP causes damage to the membrane structure and a pore is formed around the NP [27, 31, 32]. Ding and Ma identified two possible translocating pathways of Janus NPs across lipid bilayers using dissipative particle dynamics simulations [33]. Noh *et al* examined the interaction between amphiphilic NPs with striped ligands and the multicomponent lipid bilayers and found that the NPs can influence the phase separation of the lipid bilayers and the NPs eventually prefer to distribute in the liquid-disordered domains [34].

In addition, a series of experimental and simulation studies have shown that the ligand rigidity of the NPs can also affect the interaction between the NPs and lipid bilayers. NPs with different rigidities exhibit different affinities with the lipid rafts in the lipid bilayers and have different translocating pathways and velocities across the lipid bilayers [35–37]. Moreover, the NPs with the same rigidity show different interactions with the cancer cells and normal cells [38]. Therefore, the rigidity of the ligands on the surface of NPs can be changed to realize the targeted therapy of cancers in the drug design.

In a word, although plenty of studies have been performed, the influence of the physicochemical properties and distribution of ligands of the NPs on the interactions between the NPs and lipid bilayers is very complicated and the microscopic mechanism at the molecular scale is not yet well understood. In particular, the influences of the ligand density, the ratio of hydrophilic ligands to hydrophobic ligands, and the ligand rigidity of the amphiphilic NPs coated with striped ligands on their interactions with cell membranes have not been thoroughly investigated at the molecular scale.

Here, we investigated the interactions between the NPs coated with striped amphiphilic ligands and a lipid bilayer using coarse-grained molecular dynamics (MD) simulations. We mainly focus on the effects of ligand density, the ratio of hydrophilic to hydrophobic ligands, and the ligand rigidity on the interaction between the NPs and the lipid bilayer. We find that the penetration processes of the NPs can be readily regulated by changing the ligand density, the ratio of hydrophilic to hydrophobic ligands, and the ligand rigidity. Furthermore, we calculated the binding free energy of the NPs coated with different ligands with the lipid bilayer.

This work provides valuable physical insights into the microscopic mechanism governing the interactions between the amphiphilic NPs coated with striped hydrophobic/hydrophilic ligands and a lipid bilayer from both the thermodynamic and the kinetic perspectives. These insights have significant implications for efficiently regulating the interactions of the amphiphilic NPs with cellular membranes, which is important to the application of NPs in nanomedicine and the comprehension of the cytotoxicity of nanomaterials, particularly from the viewpoint of theoretical physics.

2. Methods and models

2.1. Coarse-grained simulation methods

The coarse-grained MD simulations were used to study the interactions between the NPs and the lipid bilayer. All lipids, water molecules, ions, and NPs were described using the Martini force field, which uses a 4:1 mapping scheme to coarse grain the molecules, i.e., every four non-hydrogen atoms are considered as a coarse-grained bead on average [39, 40]. In the simulations, the Lennard–Jones interaction is shifted to zero between 0.9 and 1.2 nm and the Coulomb interaction is shifted to zero between 0 and 1.2 nm. All simulations were performed using a constant particle number, pressure, and temperature ensemble. The pressures in the bilayer plane (xy-plane) and in the normal (z) direction of the bilayer were separately maintained at 1 bar (relaxation time of 12 ps) using the Parrinello-Rahman method [41, 42]. The temperature of the system was maintained at 305 K (relaxation time of 1 ps) by the velocity-rescaling method [43]. All simulations were performed with the GROMACS (version 2020.4) package with a time step of 20 fs. In order to ensure the correctness of the simulation results, no less than four sets of replicate simulations of 10 μs duration were carried out for each system after energy minimization and 20 ns equilibrium simulations.

2.2. System setup

Lipid bilayer. As shown in figure 1(a), the lipid bilayer is composed of 361 unsaturated dioctadecatrienoylphosphatidylcholine (DFPC) molecules. Each DFPC consists of a

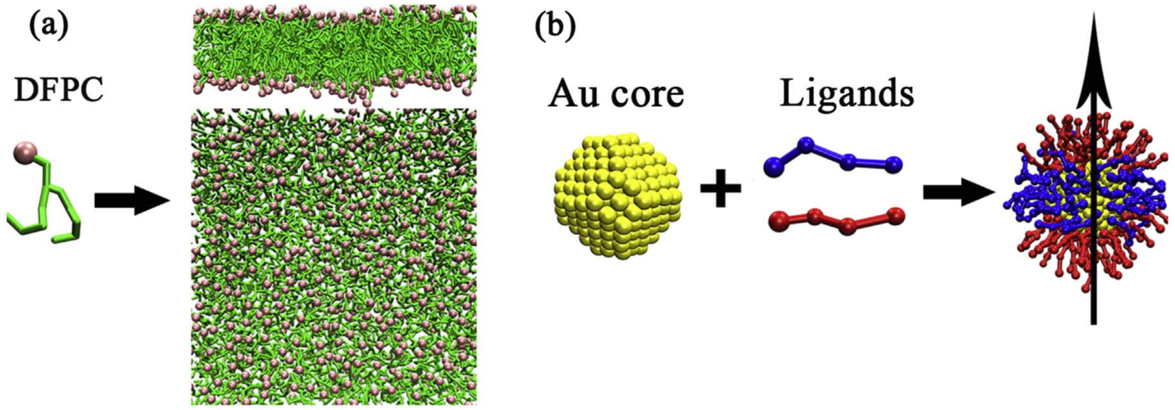

Figure 1. (a) The coarse-grained structure of DFPC lipid and the lateral and top views of a lipid bilayer composed of DFPC; (b) Schematic illustration of the AuNP coated with striped hydrophilic (red) and hydrophobic (blue) ligands. For the convenience of describing the rotation of the NP, the symmetry axis is defined by a vector passing through the center of the NP and perpendicular to the hydrophobic ligand layer.

hydrophilic headgroup and two hydrophobic tail chains, and each tail chain contains three unsaturated bonds. At the simulated temperature (305 K) in this work, DFPC is in the liquid-disordered phase.

NPs. As shown in figure 1(b), the NP is composed of a gold core and some ligands. The core was constructed in our previous work and consists of 314 C5 Martini beads arranged in a face-centered cubic structure and with a truncated octahedron shape [28]. The diameter of the core is about 2.2 nm and previous work has shown that the NP with this size is a very stable structure and can easily penetrate the lipid bilayers [44]. The core adopted a 1:1 mapping scheme, i.e., each gold atom corresponds to one C5 Martini bead. Both the neutral (hydrophobic) and charged (hydrophilic) ligands are consistent with four Martini beads and the only difference between these two kinds of ligands is their terminal beads. The terminal bead of the charged ligand is a positively charged Martini bead Qd while that of the neutral ligand is a neutral Martini bead C1. Besides the terminal beads, the other three beads in both kinds of ligands are identical and consist of two C1 beads and one N0 bead, which represents a sulfur atom grafting the ligand onto the surface of the gold core. The neutral and charged ligands correspond to the molecules of 11-mercapto-1-undecanesulfonate and 1-octanethiol, which have been widely used in previous simulations and experimental work [29, 45–57]. More details on the NP model can be found in our previous work [26, 28].

In this work, the hydrophilic and hydrophobic ligands are coated on the surface of the gold core with a striped pattern, i.e., the hydrophilic ligands are coated on the two poles of the core while the hydrophobic ligands are coated on the middle part of the surface of the core as shown in figure 1(b). We selected two different ligand grafting densities with ligand numbers of 70 and 104, corresponding to 40% and 60% surface coverage of the core [58, 59]. In addition, the rigidity of the ligands was regulated by changing the bending force constants of the bond angles between the coarse-grained beads of the ligands. Here, we examined two types of ligands with bending force constants of 25 kJ mol^{-1} and 700 kJ mol^{-1} for the bond angle [35]. For convenience, we use the symbol $NP^{r}_{m/n}$ to denote the type of NP, where m denotes the total number of ligands of the NP, n denotes the number of hydrophilic ligands, and r denotes the bending force constant of the bond angle for the ligands.

Besides DFPC and NP, there are approximately 25400 water molecules in every system. Additionally, to maintain the electrical neutrality of the systems, some chloride ions were added to each system to neutralize the positive charges carried by the NPs. The initial size of each system is about 15 $\times$ 15 $\times$ 20 nm, and the periodic boundary conditions are applied in all three directions of the systems.

2.3. Potential of mean force between the NP and the lipid bilayer

In order to reveal the microscopic mechanism of the interactions between the NPs and the lipid bilayer, we used an umbrella sampling method to calculate the potential of mean force (PMF) between the NP and the lipid bilayer. The 65 sampling windows were generated every 0.1 nm in the range of 0–6.5 nm along the z-direction from the midplane of the bilayer to the center of mass of the NP by pull simulation. In each simulation window, the distance between the center of mass of the NP and the midplane of the bilayer in the z-direction was restricted by a harmonic potential with the force constant of 1000 kJ/(mol·nm^2). The simulation time is 1 μs for each window. Finally, we used the weighted histogram analysis method to obtain the PMF profile. The difference between the maximum and minimum values of the PMF is the binding free energy between the NP and the bilayer, and the larger the binding free energy is, the tighter the particle is bound to the bilayer.

2.4. Data analysis

In order to investigate the microscopic dynamics of the interaction between the NPs and the lipid bilayer, we analyzed the contacts between NPs and the lipid bilayer at different times using the software Visual Molecular Dynamics. Additionally, in order to study the rotation of the NP during its insertion into the lipid bilayer, a vector was defined by two

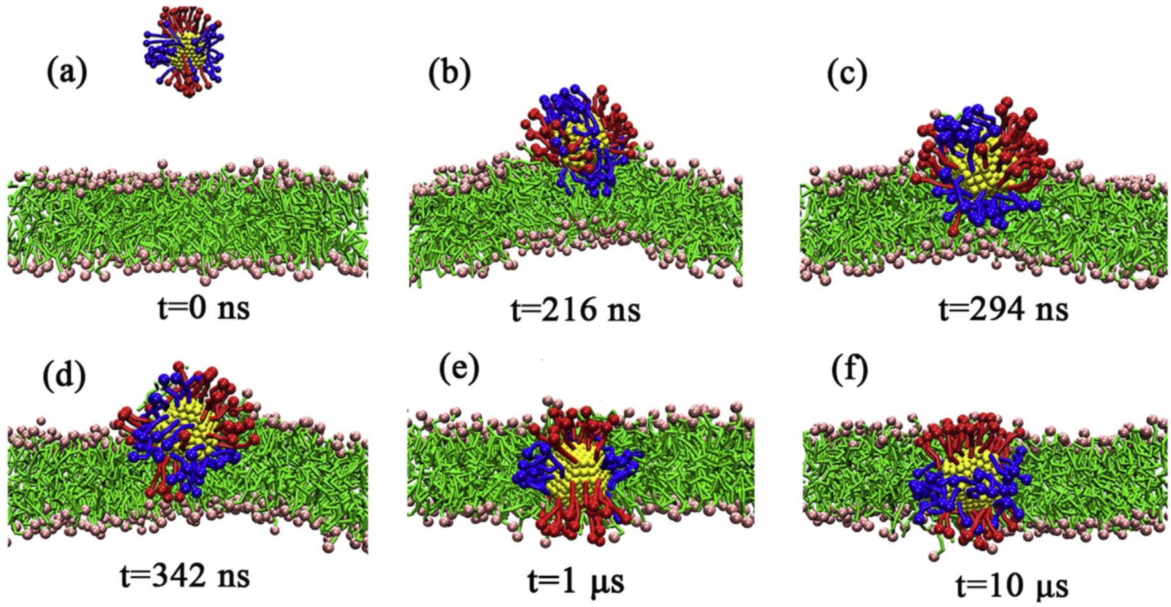

Figure 2. The kinetic process of $NP^{25}_{70/35}$ interacting with the DFPC lipid bilayer.

gold atoms in the core of the NP such that the angle between the direction of the vector and the normal direction of the lipid bilayer in the initial state of the simulation was 0°. The rotation of the NP over time was described by calculating the angle between the defined vector and the normal direction of the membrane by the *gmx gangle* tool in the GROMACS package. Furthermore, in order to quantitatively characterize the depth of the insertion of the NPs with different ratios of hydrophilic ligands and hydrophobic ligands into the lipid bilayer, we calculated the distance between the center of mass of the NP and the midplane of the bilayer in the *z*-direction.

3. Results and discussion

3.1. Effect of grafting density of ligands on the interactions between the NPs and the lipid bilayer

The grafting density of ligands on the surface of NPs can affect the effective size of the NP and further influence the interaction between the NP and lipid bilayer. To examine the effect of ligand grafting density on the interaction of the NPs with the lipid bilayer, we constructed two different NPs, i.e., $NP^{25}_{70/35}$ and $NP^{25}_{104/50}$. The total number of ligands on the surface of these two NPs is 70 and 104, respectively. The number of hydrophilic ligands is 35 and 50, respectively, and the ratio of the hydrophilic ligands to the hydrophobic ligands is about 1:1.

We first studied the interaction between $NP^{25}_{70/35}$ and the lipid bilayer. Figure 2 shows the kinetic process of $NP^{25}_{70/35}$ interacting with the DFPC bilayer. As shown in figure 2(a), in the initial state of the simulation, the NP was placed at a relatively large distance from the bilayer. At about 200 ns, the NP starts to contact the lipid bilayer and some hydrophobic ligands are inserted into the bilayer (figure 2(b)). With the increase in simulation time, more and more hydrophobic

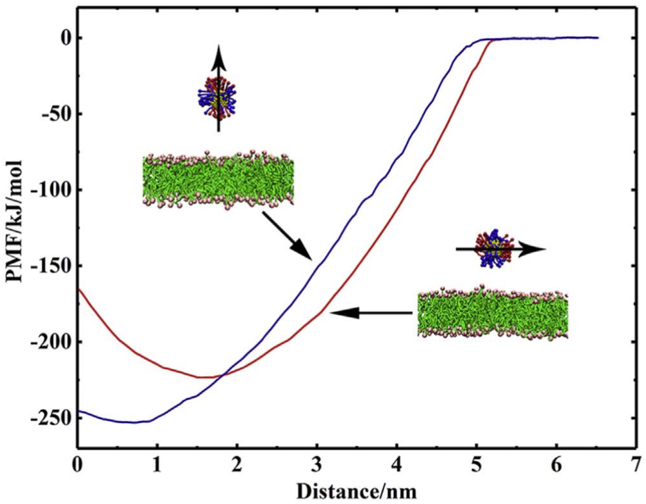

Figure 3. PMF profiles of $NP^{25}_{70/35}$ interacting with the DFPC lipid bilayer versus the distance between the center of the NP and the midplane of the lipid bilayer in the *z*-direction. Here, the blue and red curves correspond to the case of the NP inserted into the bilayer with its symmetry axis perpendicular to the bilayer plane and parallel to the bilayer plane, respectively.

ligands are inserted into the bilayer. Meanwhile, the binding state of the NP is continuously adjusted through the NP rotation, and some hydrophilic ligands are inserted into the lipid bilayer (figures 2(c) and (d)). At about 1 μs, the hydrophobic ligands of the NP were completely inserted into the hydrophobic layer of the lipid bilayer, while the hydrophilic ligands on the two poles of the NP distribute in the upper and lower hydrophilic layers of the lipid bilayer (figure 2(e)). The charged ends of the hydrophilic ligands are in contact with the head groups of the DFPC lipids, and this state maintains until the end of the 10 μs simulation (figure 2(f)). We performed four replicas of the simulations

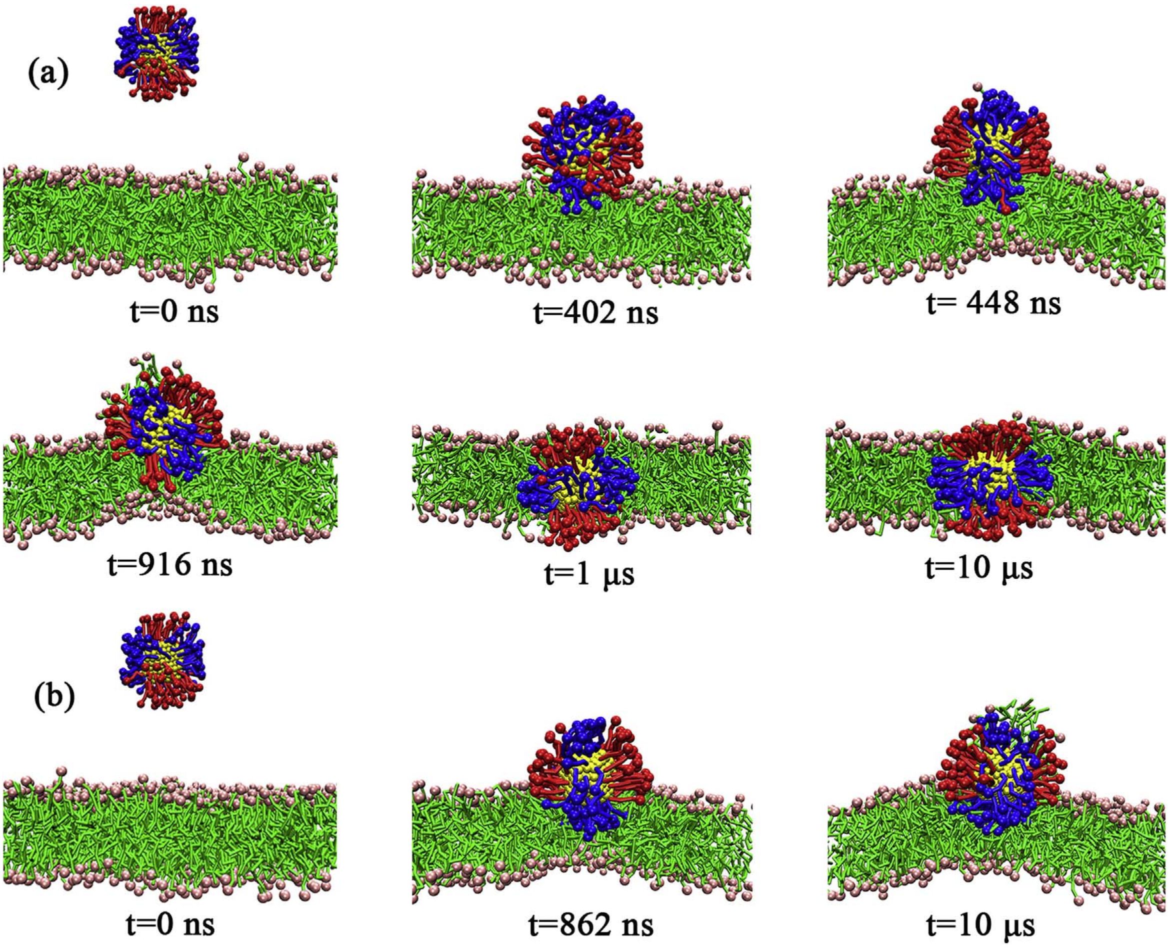

Figure 4. The kinetic processes of the insertion of $NP^{25}_{104/50}$ into the DFPC lipid bilayer (a) and adsorbed onto the surface of the lipid bilayer (b).

for this system and the results are all consistent with the NP completely embedded in the lipid bilayer as shown in figure 2(f).

To further reveal the microscopic mechanism of the interaction between $NP^{25}_{70/35}$ and the lipid bilayer, we calculated the PMF of $NP^{25}_{70/35}$ embedded in the lipid bilayer with the state of figure 2(f) (i.e., the NP symmetry axis is perpendicular to the bilayer plane). During the calculations, we imposed a restriction on the rotation of the particles, i.e., the symmetry axis of the particles was always perpendicular to the bilayer plane. The results in figure 3 show that the PMF decreases monotonically during the insertion of the NP into the DFPC bilayer. The minimum value of the PMF corresponds to the state of the center of the NP located in the midplane of the bilayer, which indicates that the insertion state of the NP in figure 2(f) is stable. In this binding state, the hydrophobic ligands of $NP^{25}_{70/35}$ are embedded in the hydrophobic layer of the lipid bilayer, avoiding contact with the water molecules; the charged ends of the hydrophilic ligands distribute in the hydrophilic layers of the lipid bilayer, without direct contact with the hydrophobic tail chains of the lipids. Therefore, this state is the optimal way to bind $NP^{25}_{70/35}$ to the lipid bilayer.

As a comparison, we also calculated the PMF between $NP^{25}_{70/35}$ and the lipid bilayer for the case with the symmetry axis of $NP^{25}_{70/35}$ parallel to the plane of the lipid bilayer (figure 3). The results show that in this case, the minimum value of the PMF does not correspond to the state of the NP center located in the midplane of the lipid bilayer, but rather at about 2 nm from the midplane of the bilayer, i.e., at the surface of the bilayer. This indicates that when the NP is bound to the membrane in this way, it is possible that the NP can only be adsorbed on the surface of the lipid bilayer. However, the binding free energy in this way is smaller than that of the way with the symmetry axis of the NP perpendicular to the bilayer plane (figure 2(f)). Therefore, in our simulations, only the insertion state shown in figure 2(f) was observed, whereas the adsorption of $NP^{25}_{70/35}$ on the surface of the lipid bilayer is absent.

Then, we investigated the interaction between $NP^{25}_{104/50}$ and the lipid bilayer. Figure 4 shows the kinetic process of the interaction of $NP^{25}_{104/50}$ with the DFPC bilayer. Unlike the case of $NP^{25}_{70/35}$, we observed two different final states of the interaction of $NP^{25}_{104/50}$ with the lipid bilayer. In the first case as shown in figure 4(a), $NP^{25}_{104/50}$ is completely embedded in the lipid bilayer in a vertical manner just as in the case of

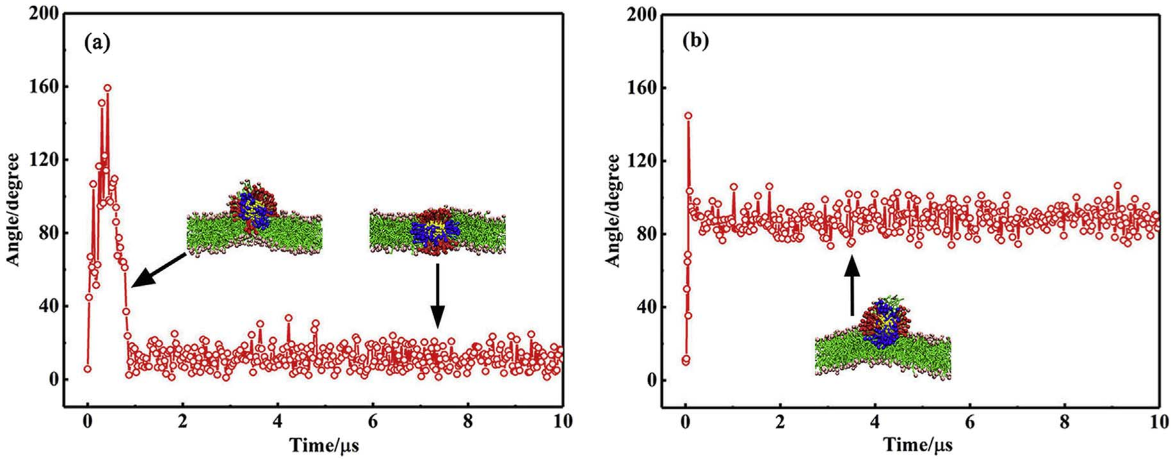

Figure 5. The variation of the angle between the symmetry axis of $NP^{25}_{104/50}$ and the normal direction of the DFPC lipid bilayer during the insertion of the NP into the lipid bilayer (a) and the adsorption of the NP on the surface of the lipid bilayer (b).

$NP^{25}_{70/35}$, and the hydrophilic and hydrophobic ligands distribute in the hydrophilic and hydrophobic layers of the lipid bilayer, respectively. In the second case as shown in figure 4(b), $NP^{25}_{104/50}$ is only partially embedded in the lipid bilayer, with its symmetry axis parallel to the bilayer plane and the hydrophilic ligands in contact with the bilayer surface. Some hydrophobic ligands are embedded in the lipid bilayer while some are exposed to water (figure 4(b)). Additionally, the lipid bilayer undergoes a certain degree of curvature due to the asymmetric insertion of the NP into the upper leaflet of the lipid bilayer.

In order to get a comprehensive understanding of the adjustment process of $NP^{25}_{104/50}$ on the surface of the lipid bilayer and the stability of the different binding states of the NP to the lipid bilayer, we examined the rotation of $NP^{25}_{104/50}$ during its insertion into the lipid bilayer or adsorption on the surface of the lipid bilayer. As shown in figure 5, in the first interaction process, $NP^{25}_{104/50}$ first contacts the lipid bilayer in a perpendicular manner (i.e. the hydrophilic ligand contacts the lipid bilayer first), and after about 1 μs of the adjustment on the bilayer surface, it is completely inserted into the lipid bilayer and reaches a stable state. In the second interaction process, $NP^{25}_{104/50}$ is stabilized on the bilayer surface with the symmetry axis parallel to the bilayer plane almost without rotational adjustment until the end of the simulation. Therefore, the results in figure 5 indicate that both binding states of $NP^{25}_{104/50}$ to the lipid bilayer shown in figure 4 are relatively stable. In addition, the initial contacting state is an important factor in determining the final binding state of the NP with the lipid bilayer.

Furthermore, the PMF of $NP^{25}_{104/50}$ interacting with the lipid bilayer was calculated (figure 6). The results show that the binding free energies for the two interaction states of $NP^{25}_{104/50}$ with the lipid bilayer are approximately identical in magnitude, which means that the NP can both be stably adsorbed on the bilayer surface and be stably embedded in the lipid bilayer (as shown in figure 4). When the NP is inserted into the bilayer, it is inevitably accompanied by the bending of the ligands and the rearrangement of lipid molecules in the bilayer. For $NP^{25}_{70/35}$, the ligand density is relatively low and the spacing between the ligands is relatively large. Therefore, the ligands can be bent and adjusted relatively freely during the insertion of $NP^{25}_{70/35}$. Additionally, the effective size of $NP^{25}_{70/35}$ is relatively small and thus the lipid packing in the bilayer does not need to be adjusted drastically during the process of the insertion of the NP into the bilayer. Therefore, $NP^{25}_{70/35}$ can be easily embedded into the bilayer. On the contrary, for $NP^{25}_{104/50}$, as the number of ligands increases, the spacing between the ligands becomes smaller and the degree of freedom of ligand bending is restricted during the process of the insertion of the NP into the bilayer, which indicates that the insertion of $NP^{25}_{104/50}$ into the bilayer will cause a large deformation of the ligands and increase the free energy of the system. Additionally, as the density of the ligands increases, the effective size of $NP^{25}_{104/50}$ increases and the insertion of the NP into the bilayer will cause a large adjustment of lipid packing, which will also increase the free energy of the system. Therefore, the PMF of $NP^{25}_{104/50}$ adsorbed on the bilayer

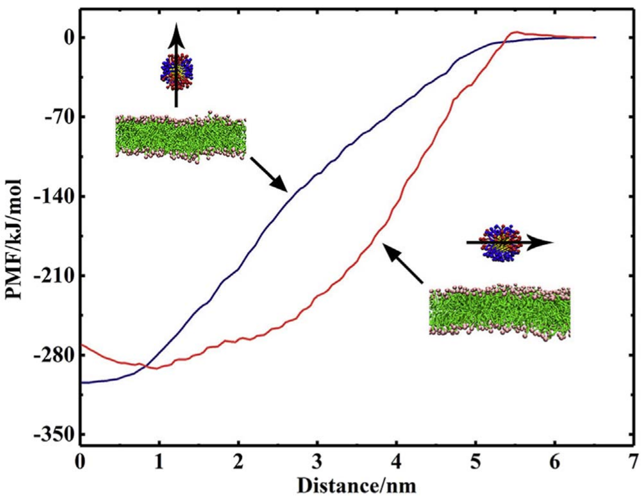

Figure 6. PMF profiles for the two different interactions of $NP^{25}_{104/50}$ with the DFPC lipid bilayer.

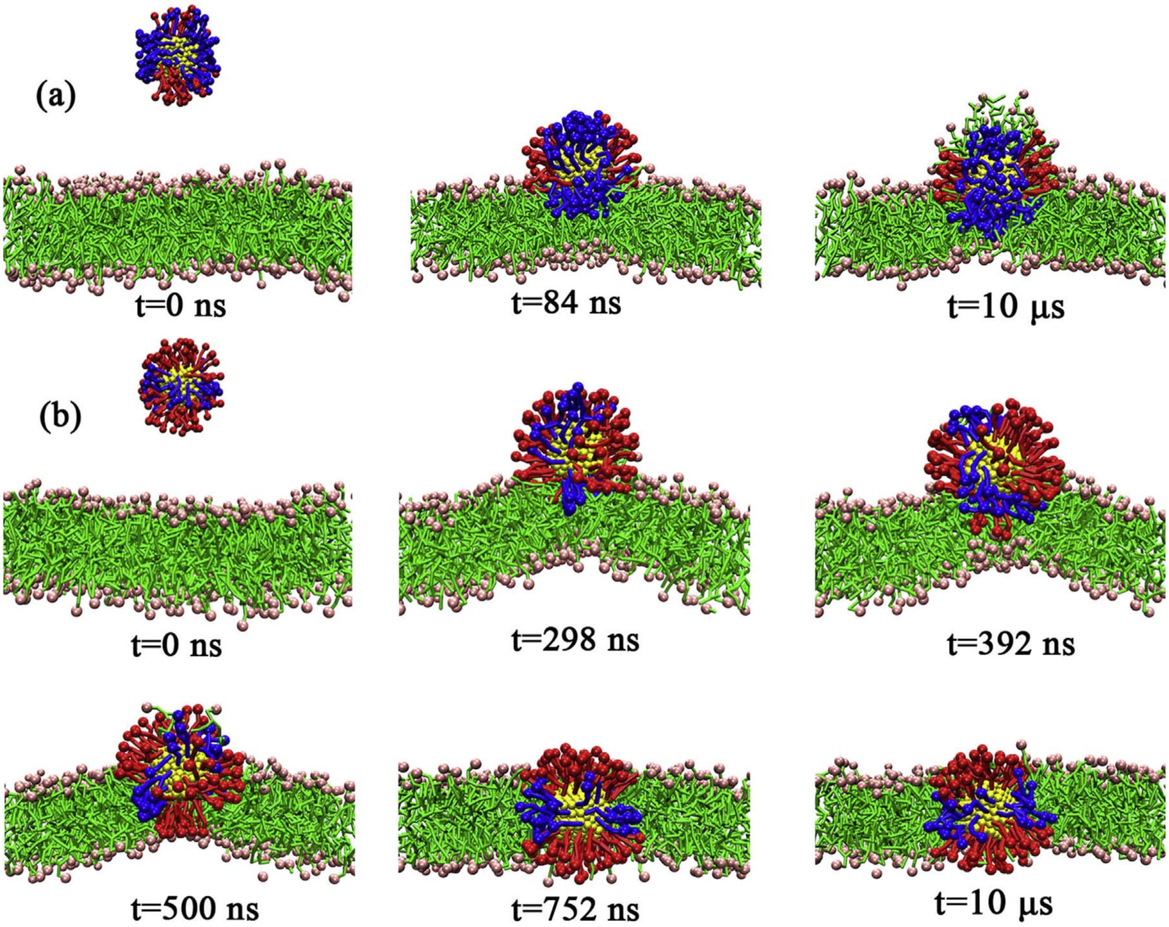

Figure 7. The kinetic processes of the interactions of $NP^{25}_{104/30}$ (a) and $NP^{25}_{104/70}$ (b) with the DFPC lipid bilayer.

surface and the PMF of $NP^{25}_{104/50}$ embedded in the bilayer are approximately identical, i.e., $NP^{25}_{104/50}$ may either be embedded in the bilayer or be adsorbed on the bilayer surface (as shown in figure 4).

3.2. Effect of the ratio of hydrophobic ligands on the interaction of the NP with the lipid bilayer

Next, we investigated the effect of the ratio of hydrophilic ligands to the hydrophobic ligands on the interaction between the NP and the DFPC bilayer. We changed the ratios of hydrophilic ligands to hydrophobic ligands of the NP from 1:1 for the $NP^{25}_{104/50}$ studied above to 1:2 and 2:1 and denoted the NPs by the symbols $NP^{25}_{104/30}$ and $NP^{25}_{104/70}$, respectively.

Figure 7 shows the kinetics of the interaction of $NP^{25}_{104/30}$ and $NP^{25}_{104/70}$ with the DFPC bilayer. For the $NP^{25}_{104/30}$ as shown in figure 7(a), the hydrophobic ligands start to insert into the membrane at 84 ns and the NP is partially inserted into the bilayer. This state remains until the end of the simulation. Throughout the simulation, no obvious rotation of the NP is observed. For $NP^{25}_{104/70}$ as shown in figure 7(b), due to the relatively small number of hydrophobic ligands, only a few ligands are inserted into the bilayer in the initial contacting state (298 ns), and most of the volume of the NP is in water (not shown). After a period of rotation and adjustment, the NP is fully embedded in the bilayer at 752 ns.

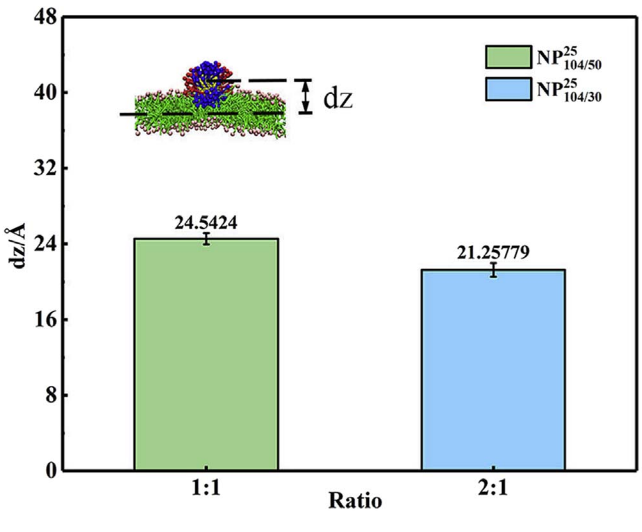

Figure 8. The distance between the centers of mass for $NP^{25}_{104/50}$ and $NP^{25}_{104/30}$ and the midplane of the DFPC lipid bilayer in the *z*-direction.

Comparing these two interacting processes, we find that the number of hydrophobic ligands and the rotation of the NP

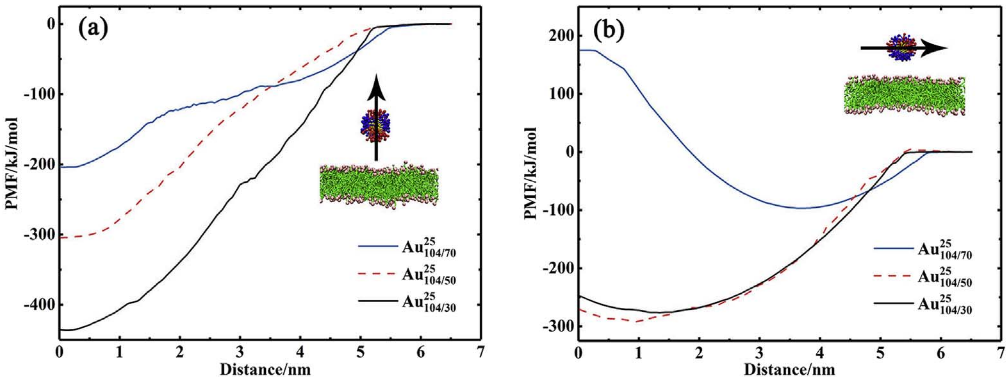

Figure 9. PMF curves for $NP^{25}_{104/70}$, $NP^{25}_{104/50}$, and $NP^{25}_{104/30}$ with their symmetry axes perpendicular to the DFPC bilayer plane (a) and parallel to the DFPC bilayer plane (b).

play a key role in the interaction of NP with the bilayer. For $NP^{25}_{104/30}$, the number of hydrophobic ligands is large, and once the NP is in contact with the bilayer, a large number of hydrophobic ligands will be inserted into the membrane, making the NP adsorb onto the surface of the bilayer stably and restricting the rotation of $NP^{25}_{104/30}$ on the bilayer surface. On the contrary, for $NP^{25}_{104/70}$, the number of hydrophobic ligands is relatively small, and even if these ligands are inserted into the bilayer, they are not able to stably anchor the NP on the bilayer surface. Therefore, the binding state of $NP^{25}_{104/70}$ will be continuously adjusted, and the hydrophilic ligands will be gradually inserted into the bilayer, resulting in the complete insertion of $NP^{25}_{104/70}$ into the bilayer as shown in figure 7(b).

Figure 8 compares the distance between the center of $NP^{25}_{104/50}$ and the midplane of the DFPC bilayer (figure 4(b)) with the distance between the center of $NP^{25}_{104/30}$ and the midplane of the bilayer (figure 7(a)) in z-direction. The result shows that the distance between the center of $NP^{25}_{104/30}$ and the midplane of the bilayer is smaller than the distance between the center of $NP^{25}_{104/50}$ and the midplane of the bilayer, indicating that the depth of the NP inserted into the bilayer increases with the increase of the number of hydrophobic ligands. Therefore, the increase of hydrophobic ligands makes the NP adsorb more tightly on the bilayer surface.

In addition, we also compared the PMFs of the interactions of $NP^{25}_{104/70}$, $NP^{25}_{104/50}$, and $NP^{25}_{104/30}$ with the bilayer for the case with the symmetry axis of the NP perpendicular to the bilayer plane and parallel to the bilayer plane, respectively, as shown in figure 9. For the case of the symmetry axis of the NP perpendicular to the bilayer plane as shown in figure 9(a), the minimum value of PMF increases with the increase of the number of hydrophilic ligands, i.e., the binding free energy of $NP^{25}_{104/70}$ is the smallest one while that of $NP^{25}_{104/30}$ is the largest one. This is because when the NP is fully inserted into the bilayer with its symmetry axis perpendicular to the bilayer plane, some of the hydrophilic ligands will also be inserted into the hydrophobic layer of the bilayer, and these hydrophilic ligands are in contact with the hydrophobic tail chains of DFPCs, increasing the free energy of the system. Consequently, by increasing the hydrophilic ligands, the number of the hydrophilic ligands inserted into the bilayer correspondingly increases and the binding free energy decreases.

For the case of the symmetry axis of the NP parallel to the bilayer plane as shown in figure 9(b), the PMF minimum values for $NP^{25}_{104/30}$ and $NP^{25}_{104/50}$ are comparable and they are much smaller than the PMF minimum value for $NP^{25}_{104/70}$. However, the PMF minimum values for all the three NPs in this case are larger than the PMF minimum values for the NPs in the case of the NP symmetry axis perpendicular to the bilayer plane (figure 9(a)), respectively. Therefore, the complete insertion of the NPs into the bilayer with their symmetry axis parallel to the bilayer plane was never observed in the unbiased simulations. Additionally, for $NP^{25}_{104/30}$, the binding free energy with its symmetry axis perpendicular to the bilayer plane is much larger than the binding free energy with its symmetry axis parallel to the bilayer plane, implying that $NP^{25}_{104/30}$ can be completely inserted into the bilayer with its symmetry axis perpendicular to the bilayer plane. However, as mentioned above, due to the large number of the hydrophobic ligands, the rotation of $NP^{25}_{104/30}$ is restrained at the initial contacting stage. Therefore, although the complete insertion of $NP^{25}_{104/30}$ is thermodynamically favorable, it is kinetically unfavorable. Therefore, the complete insertion of $NP^{25}_{104/30}$ into the bilayer with its symmetry axis perpendicular to the bilayer plane is absent in the unbiased simulation.

3.3. Effect of ligand rigidity on the interaction between the NP and the lipid bilayer

Finally, we examined the effect of ligand rigidity on the interaction between the NP and the DFPC bilayer. We increase the bending force constant of the bond angle for the ligands of the above studied $NP^{25}_{104/70}$ from 25 kJ mol^{-1} to 700 and denoted the NP as $NP^{700}_{104/70}$.

The kinetic process of the insertion of $NP^{700}_{104/70}$ into the lipid bilayer is shown in figure 10. Compared with the process of the insertion of $NP^{25}_{104/70}$ into the bilayer as shown in figure 7(b), the insertion of $NP^{700}_{104/70}$ into the bilayer is much slower. $NP^{25}_{104/70}$ starts to contact the bilayer at about 300 ns and is completely inserted into the bilayer at about 750 ns,

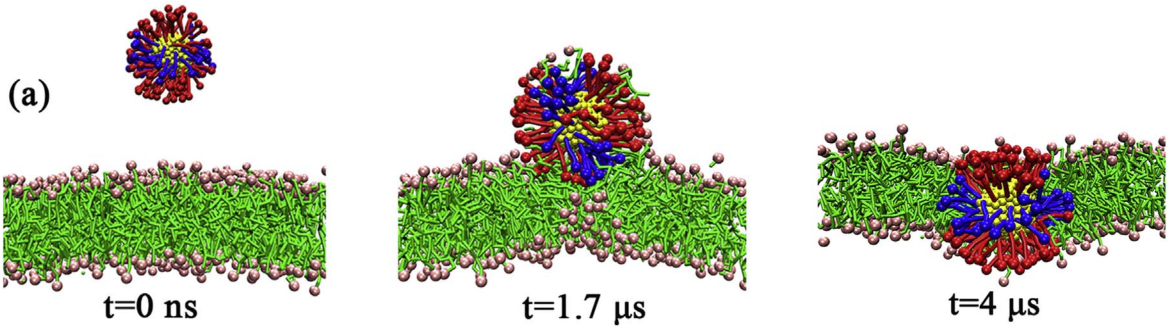

Figure 10. The kinetic process of the insertion of $NP^{700}_{104/70}$ into the DFPC lipid bilayer.

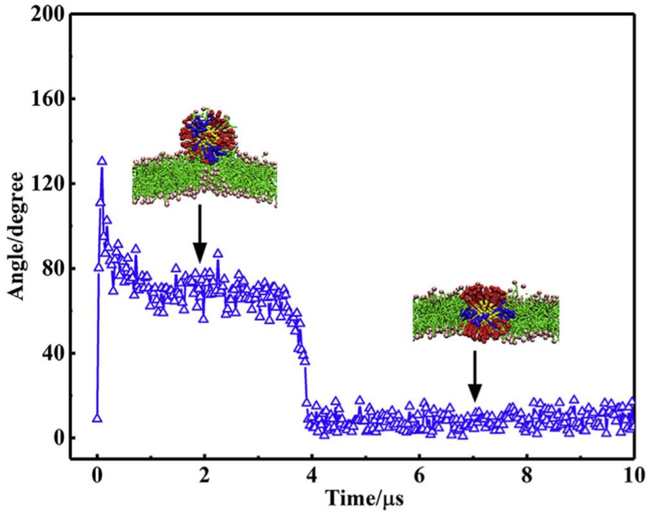

Figure 11. The variation of the angle between the symmetry axis of $NP^{700}_{104/70}$ and the normal direction of the DFPC lipid bilayer during the insertion of the NP into the lipid bilayer.

whereas $NP^{700}_{104/70}$ does not contact the bilayer until 1.7 μs and is completely inserted into the bilayer at about 4 μs. Figure 11 shows the rotation of $NP^{700}_{104/70}$ during its insertion into the bilayer. The results show that $NP^{700}_{104/70}$ reaches a stable state until about 4 μs. These results indicate that the increased rigidity of the ligand not only makes the NP difficult to be adsorbed to the surface of the bilayer, but also slows down the velocity of the insertion of the NP into the bilayer.

4. Conclusion

In this work, we investigated the interactions between the amphiphilic NPs with a stripe-like distribution of hydrophilic/hydrophobic ligands and the DFPC lipid bilayer using coarse-grained MD simulations. By examining the effects of ligand density and ligand rigidity on the interaction between the NPs and the bilayer, we find that both of these factors regulate the interactions between the NPs and the bilayer by affecting the deformation and the degree of freedom of the adjustment of ligands. With the increase in ligand density and rigidity, the degree of freedom of ligand deformation and adjustment decreases, and it is more difficult for the NPs to be completely inserted into the bilayer; on the contrary, with lower ligand density and smaller rigidity, the degree of freedom of ligand deformation is higher, and when interacting with the bilayer, the configuration of the ligands can be easily adjusted so that the NP is more easily completely embedded in the bilayer. In addition, by adjusting the ratio of the hydrophobic ligands to the hydrophilic ligands, we find that the hydrophobic ligands play a key role in the interaction of the NPs with the bilayer. When the ratio of the hydrophobic ligands to the hydrophilic ligands is relatively large, once the NP contacts the bilayer, plenty of hydrophobic ligands are inserted into the bilayer, which restrains the NP rotation and the NP can only be partially inserted into the bilayer. However, when the ratio is relatively small, the insertion of hydrophobic ligands is not able to completely restrain the NP rotation; thus, the NP can be completely embedded in the bilayer eventually. Therefore, the NP rotation on the bilayer surface plays a very important role in the kinetic process of the insertion of the NP into the bilayer. This work provides a feasible scheme for tuning the interaction between the amphiphilic NPs and the biological membranes by changing the properties of the ligands coated on the surface of the NPs and is helpful in the application of amphiphilic NPs in the relevant fields such as nanomedicine.

Acknowledgments

This work was supported by the National Natural Science Foundation of China (Grant No. 11 674 287), and the Zhejiang Provincial Natural Science Foundation of China (Grant No. LY19A040009).

References

[1] Chen G, Roy I, Yang C and Prasad P N 2016 Nanochemistry and nanomedicine for nanoparticle-based diagnostics and therapy *Chem. Rev.* **116** 2826

[2] Smith B R and Gambhir S S 2017 Nanomaterials for *in vivo* imaging *Chem. Rev.* **117** 901

[3] Bogart L K, Pourroy G, Murphy C J, Puntes V, Pellegrino T, Rosenblum D, Peer D and Lévy R 2014 Nanoparticles for imaging, sensing, and therapeutic intervention *ACS Nano* **8** 3107

[4] Ding H-M and Ma Y-Q 2015 Theoretical and computational investigations of nanoparticle-biomembrane interactions in cellular delivery *Small* **11** 1055

[5] Yang K and Ma Y-Q 2010 Computer simulation of the translocation of nanoparticles with different shapes across a lipid bilayer *Nat. Nanotechnol.* **5** 579

[6] Strachan J B, Dyett B P, Nasa Z, Valery C and Conn C E 2020 Toxicity and cellular uptake of lipid nanoparticles of different structure and composition *J. Colloid Interface Sci.* **576** 241

[7] Luk B T, Hu C-M J, Fang R H, Dehaini D, Carpenter C, Gao W and Zhang L 2014 Interfacial interactions between natural RBC membranes and synthetic polymeric nanoparticles *Nanoscale* **6** 2730

[8] Geng J, Sun C, Liu J, Liao L D, Yuan Y, Thakor N, Wang J and Liu B 2015 Biocompatible conjugated polymer nanoparticles for efficient photothermal tumor therapy *Small* **11** 1603

[9] Miller K P, Wang L, Benicewicz B C and Decho A W 2015 Inorganic nanoparticles engineered to attack bacteria *Chem. Soc. Rev.* **44** 7787

[10] Yang X, Yang M, Pang B, Vara M and Xia Y 2015 Gold nanomaterials at work in biomedicine *Chem. Rev.* **115** 10410

[11] Boisselier E and Astruc D 2009 Gold nanoparticles in nanomedicine: preparations, imaging, diagnostics, therapies and toxicity *Chem. Soc. Rev.* **38** 1759

[12] Sperling R A, Gil P R, Zhang F, Zanella M and Parak W J 2008 Biological applications of gold nanoparticles *Chem. Soc. Rev.* **37** 1896

[13] Yeh Y-C, Creran B and Rotello V M 2012 Gold nanoparticles: preparation, properties, and applications in bionanotechnology *Nanoscale* **4** 1871

[14] Sharifi S, Behzadi S, Laurent S, Forrest M L, Stroeve P and Mahmoudi M 2012 Toxicity of nanomaterials *Chem. Soc. Rev.* **41** 2323

[15] Sani A, Cao C and Cui D 2021 Toxicity of gold nanoparticles (AuNPs): a review *Biochem. Biophys. Rep.* **26** 100991

[16] Malhotra N, Lee J-S, Liman R A D, Ruallo J M S, Villaflores O B, Ger T-R and Hsiao C-D 2020 Potential toxicity of iron oxide magnetic nanoparticles: a review *Molecules* **25** 3159

[17] Medici S, Peana M, Pelucelli A and Zoroddu M A 2021 Au updated overview on metal nanoparticles toxicity *Semin. Cancer Biol.* **76** 17

[18] Saei A A, Yazdani M, Lohse S E, Bakhtiary Z, Serpooshan V, Ghavami M, Asadian M, Mashaghi S, Dreaden E C and Mashaghi A 2017 Nanoparticle surface functionality dictates cellular and systemic toxicity *Chem. Mater.* **29** 6578

[19] Kim S T, Saha K, Kim C and Rotello V M 2013 The role of surface functionality in determining nanoparticle cytotoxicity *Acc. Chem. Res.* **46** 681

[20] Mout R, Moyano D F, Rana S and Rotello V M 2012 Surface functionalization of nanoparticles for nanomedicine *Chem. Soc. Rev.* **41** 2539

[21] Arvizo R R, Miranda O R, Thompson M A, Pabelick C M, Bhattacharya R, Robertson J D, Rotello V M, Prakash Y and Mukherjee P 2010 Effect of nanoparticle surface charge at the plasma membrane and beyond *Nano Lett.* **10** 2543

[22] Guo Y, Terazzi E, Seemann R, Fleury J B and Baulin V A 2016 Direct proof of spontaneous translocation of lipid-covered hydrophobic nanoparticles through a phospholipid bilayer *Sci. Adv.* **2** e1600261

[23] Lunnoo T, Assawakhajornsak J and Puangmali T 2019 *In silico* study of gold nanoparticle uptake into a mammalian cell: interplay of size, shape, surface charge, and aggregation *J. Phys. Chem.* C **123** 3801

[24] Cho E C, Xie J, Wurm P A and Xia Y 2009 Understanding the role of surface charges in cellular adsorption versus internalization by selectively removing gold nanoparticles on the cell surface with a I2/KI etchant *Nano Lett.* **9** 1080

[25] Jing B and Zhu Y 2011 Disruption of supported lipid bilayers by semihydrophobic nanoparticles *J. Am. Chem. Soc.* **133** 10983

[26] Liang Y-R and Liang Q 2019 Molecular simulation of interaction between charged nanoparticles and phase-separated biomembranes containing charged lipids *Acta Phys. Sin.* **68** 028701

[27] Lee K, Zhang L, Yi Y, Wang X and Yu Y 2018 Rupture of lipid membranes induced by amphiphilic Janus nanoparticles *ACS Nano* **12** 3646

[28] Chen X, Tieleman D P and Liang Q 2018 Modulating interactions between ligand-coated nanoparticles and phase-separated lipid bilayers by varying the ligand density and the surface charge *Nanoscale* **10** 2481

[29] Van Lehn R C, Atukorale P U, Carney R P, Yang Y-S, Stellacci F, Irvine D J and Alexander-Katz A 2013 Effect of particle diameter and surface composition on the spontaneous fusion of monolayer-protected gold nanoparticles with lipid bilayers *Nano Lett.* **13** 4060

[30] Verma A, Uzun O, Hu Y, Han H, Watson N, Chen S, Irvine D and Stellacci F 2008 Surface-structure-regulated cell-membrane penetration by monolayer-protected nanoparticles *Nat. Mater.* **7** 588

[31] Lee K and Yu Y 2019 Lipid bilayer disruption induced by amphiphilic Janus nanoparticles: The non-monotonic effect of charged lipids *Soft Matter* **15** 2373

[32] Lee K and Yu Y 2018 Lipid bilayer disruption by amphiphilic Janus nanoparticles: the role of Janus balance *Langmuir* **34** 12387

[33] Ding H-M and Ma Y-Q 2012 Interactions between Janus particles and membranes *Nanoscale* **4** 1116

[34] Noh S Y, Nash A and Notman R 2020 The aggregation of striped nanoparticles in mixed phospholipid bilayers *Nanoscale* **12** 4868

[35] Lin X and Lin X 2021 Surface ligand rigidity modulates lipid raft affinity of ultra-small hydrophobic nanoparticles: Insights from molecular dynamics simulations *Nanoscale* **13** 9825

[36] Wang S, Guo H, Li Y and Li X 2019 Penetration of nanoparticles across a lipid bilayer: effects of particle stiffness and surface hydrophobicity *Nanoscale* **11** 4025

[37] He J, Pang W, Gu B, Lin X and Ye J 2022 The stiffness-dependent tumor cell internalization of liquid metal nanoparticles *Nanoscale* **14** 16902

[38] Cong V T, Houng J L, Kavallaris M, Chen X, Tilley R D and Gooding J J 2022 How can we use the endocytosis pathways to design nanoparticle drug-delivery vehicles to target cancer cells over healthy cells? *Chem. Soc. Rev.* **51** 7531

[39] Marrink S J, De Vries A H and Mark A E 2004 Coarse grained model for semiquantitative lipid simulations *J. Phys. Chem.* B **108** 750

[40] Marrink S J and Tieleman D P 2013 Perspective on the Martini model *Chem. Soc. Rev.* **42** 6801

[41] Parrinello M and Rahman A 1981 Polymorphic transitions in single crystals: A new molecular dynamics method *J. Appl. Phys.* **52** 7182

[42] Nosé S and Klein M 1983 Constant pressure molecular dynamics for molecular systems *Mol. Phys.* **50** 1055

[43] Bussi G, Donadio D and Parrinello M 2007 Canonical sampling through velocity rescaling *J. Chem. Phys.* **126** 014101

[44] Oh E, Delehanty J B, Sapsford K E, Susumu K, Goswami R, Blanco-Canosa J B, Dawson P E, Granek J, Shoff M and Zhang Q 2011 Cellular uptake and fate of PEGylated gold nanoparticles is dependent on both cell-penetration peptides and particle size *ACS Nano* **5** 6434

[45] Van Lehn R C and Alexander-Katz A 2014 Free energy change for insertion of charged, monolayer-protected nanoparticles into lipid bilayers *Soft Matter* **10** 648
[46] Van Lehn R C and Alexander-Katz A 2014 Fusion of ligand-coated nanoparticles with lipid bilayers: effect of ligand flexibility *J. Phys. Chem.* A **118** 5848
[47] Van Lehn R C, Ricci M, Silva P H, Andreozzi P, Reguera J, Voïtchovsky K, Stellacci F and Alexander-Katz A 2014 Lipid tail protrusions mediate the insertion of nanoparticles into model cell membranes *Nat. Commun.* **5** 4482
[48] Van Lehn R C and Alexander-Katz A 2015 Pathway for insertion of amphiphilic nanoparticles into defect-free lipid bilayers from atomistic molecular dynamics simulations *Soft Matter* **11** 3165
[49] Van Lehn R C and Alexander-Katz A 2017 Grafting charged species to membrane-embedded scaffolds dramatically increases the rate of bilayer flipping *ACS Cent. Sci.* **3** 186
[50] Lin J, Zhang H, Chen Z and Zheng Y 2010 Penetration of lipid membranes by gold nanoparticles: insights into cellular uptake, cytotoxicity, and their relationship *ACS Nano* **4** 5421
[51] Lin J-Q, Zheng Y-G, Zhang H-W and Chen Z 2011 A simulation study on nanoscale holes generated by gold nanoparticles on negative lipid bilayers *Langmuir* **27** 8323
[52] Lin J and Alexander-Katz A 2013 Cell membranes open 'doors' for cationic nanoparticles/biomolecules: insights into uptake kinetics *ACS Nano* **7** 10799
[53] Simonelli F, Bochicchio D, Ferrando R and Rossi G 2015 Monolayer-protected anionic Au nanoparticles walk into lipid membranes step by step *J. Phys. Chem. Lett.* **6** 3175
[54] Angelikopoulos P, Sarkisov L, Cournia Z and Gkeka P 2017 Self-assembly of anionic, ligand-coated nanoparticles in lipid membranes *Nanoscale* **9** 1040
[55] Gkeka P, Angelikopoulos P, Sarkisov L and Cournia Z 2014 Membrane partitioning of anionic, ligand-coated nanoparticles is accompanied by ligand snorkeling, local disordering, and cholesterol depletion *PLoS Comput. Biol.* **10** e1003917
[56] Gkeka P, Sarkisov L and Angelikopoulos P 2013 Homogeneous hydrophobic-hydrophilic surface patterns enhance permeation of nanoparticles through lipid membranes *J. Phys. Chem. Lett.* **4** 1907
[57] Heikkilä E, Martinez-Seara H, Gurtovenko A A, Vattulainen I and Akola J 2014 Atomistic simulations of anionic Au144 (SR) 60 nanoparticles interacting with asymmetric model lipid membranes *Biochim. Biophys. Acta Biomembr.* **1838** 2852
[58] Jackson A M, Hu Y, Silva P J and Stellacci F 2006 From homoligand-to-mixed-ligand-monolayer-protected metal nanoparticles: A scanning tunneling microscopy investigation *J. Am. Chem. Soc.* **128** 11135
[59] Verma A, Uzun O, Hu Y, Hu Y, Han H-S, Watson N, Chen S, Irvine D J and Stellacci F 2008 Surface-structure-regulated cell-membrane penetration by monolayer-protected nanoparticles *Nat. Mater.* **7** 588